UCRL-JRNL-200174

Excitations, Optical Absorption Spectra, and Optical Excitonic Gaps of Heterofullerenes: I. C_{60}, $C_{59}N^+$ and $C_{48}N_{12}$

Rui-Hua Xie, Garnett W. Bryant, Guangyu Sun, Mark C. Nicklaus, David Heringer, Th. Frauenheim, M. Riad Manaa, Vedene H. Smith, Jr., Yasuyuki Araki and Osamu Ito

October 8, 2003

Journal of Chemical Physics

DISCLAIMER

This work was performed under the auspices of the U.S. Department of Energy by the University of California, Lawrence Livermore National Laboratory under Contract No. W-7405-Eng-48.

Excitations, optical absorption spectra, and optical excitonic gaps of heterofullerenes: I. C_{60}, $C_{59}N^+$ and $C_{48}N_{12}$

Rui-Hua Xie and Garnett W. Bryant
National Institute of Standards and Technology, Gaithersburg, MD 20899-8423, USA

Guangyu Sun and Mark C. Nicklaus
Laboratory of Medicinal Chemistry, NCI-Frederick, NIH, Frederick, MD 21702, USA

David Heringer and Th. Frauenheim
Department of Theoretical Physics, University of Paderborn, D-33098 Paderborn, Germany

M. Riad Manaa
University of California, Lawrence Livermore National Laboratory, Energetic Materials Center, 7000 East Avenue, P.O.Box 808, L-282 Livermore, CA 95441, USA

Vedene H. Smith, Jr.
Department of Chemistry, Queen's University, Kingston, ON K7L 3N6, Canada

Yasuyuki Araki and Osamu Ito
Institute of Multidisciplinary Research for Advanced Materials, Tohoku University, Sendai 980-8577, Japan

(August 14, 2003)

Low-energy excitations and optical absorption spectrum of C_{60} are computed by using time-dependent (TD) Hartree-Fock (HF), TD-density functional theory (TD-DFT), TD DFT-based tight-binding (TD-DFT-TB) and a semiempirical ZINDO method. A detailed comparison of experiment and theory for the excitation energies, optical gap and absorption spectrum of C_{60} is presented. It is found that electron correlations and collective effects of exciton pairs play important roles in assigning accurately the spectral features of C_{60} and the TD-DFT method with non-hybrid functionals or a local spin density approximation leads to more accurate excitation energies than with hybrid functionals. The level of agreement between theory and experiment for C_{60} justifies similar calculations of the excitations and optical absorption spectrum of a monomeric azafullerene cation $C_{59}N^+$, to serve as a reference for the characterization of carborane anion salts. Although it is an isoelectronic analogue to C_{60}, $C_{59}N^+$ exhibits distinguishing spectral features different from C_{60}: (1) the first singlet is dipole-allowed and the optical gap is redshifted by 1.44 eV; (2) several weaker absorption maxima occur in the visible region; (3) the transient triplet-triplet absorption at 1.60 eV (775 nm) is much broader and the decay of the triplet state is much faster. The calculated spectra of $C_{59}N^+$ characterize and explain well our measured ultraviolet-visible (UV-vis) and transient absorption spectra of the carborane anion salt $[C_{59}N][Ag(CB_{11}H_6Cl_6)_2]$ [K.C. Kim, F. Hauke, A. Hirsch, P.D.W. Boyd, E. Carter, R.S. Armstrong, P.A. Lay, and C.A. Reed, J. Am. Chem. Soc. **125**, 4024 (2003)]. For the most stable isomer of $C_{48}N_{12}$, we predict that the first singlet is dipole-allowed, the optical gap is redshifted by 1.22 eV relative to that of C_{60}, and optical absorption maxima occur at 585, 528, 443, 363, 340, 314 and 303 nm . We point out that the characterization of the UV-vis and transient absorption spectra of $C_{48}N_{12}$ isomers is helpful in distinguishing the isomer structures required for applications in molecular electronics. For $C_{59}N^+$ and $C_{48}N_{12}$ as well as C_{60}, the TD-DFT-TB yields reasonable agreement with TD-DFT calculations at a highly reduced cost. Our study suggests that C_{60}, $C_{59}N^+$ and $C_{48}N_{12}$, which differ in their optical gaps, may have potential applications in polymer science, biology and medicine as single-molecule fluorescent probes.

PACS (numbers): 32.30. Jc, 33.20.-t, 36.20.Kd, 71.15.Mb

I. INTRODUCTION

Since the discovery of C_{60} [1], doped fullerenes have been of great interest due to their remarkable structural, electronic, optical and magnetic properties [2–5]. For example, doped fullerenes can be superconducting [2], exhibit large third-order optical nonlinearities [3], and be ideal candidates as photonic devices [4] such as all-optical switching, data processing, and optical limiting (eye and sensor protections). There are three doping methods of permanently altering the charge distribution and electronic structures of the par-

ent fullerenes: the introduction of dopant species surrounding the fullerene, the inclusion of atoms or ions inside the fullerene cage, and the substitution of one or more of the carbon atoms with dopants. In this work, we focus on *heterofullerenes* [2] formed by the substitutional doping method.

The substitutional doping of a nitrogen atom into the fullerene strongly influences the structural, electronic and physical properties of the parent fullerene [6]. Hummelen *et al.* [7] synthesized $C_{59}N^+$ (an isoelectronic analogue to C_{60}) efficiently in the gas phase. Reed and coworkers [8] have recently reported that the monomeric $C_{59}N^+$ cation can be isolated as a carborane anion salt. The simplest azafullerene, $C_{59}N$ (a resulting azafullerene radical, and a highly reactive species), has been synthesized in macroscopic quantity [9,10]. Meanwhile, the bulk preparation of hydroazafullerene $C_{59}HN$, the simplest closed-shell azafullerene, was reported [11]. This azafullerene is of special interest because the spectroscopic properties of $C_{59}HN$ can be useful as a reference for the characterization of more complex derivatives, for example, the dimer $(C_{59}N)_2$ [7], $C_{59}(CHPh_2)N$ [12], $C_{59}(C_6H_4CH_3)N$ [13], $C_{59}(C_6H_4OCH_3)N$ [13], $C_{59}(C_{10}H_6Cl)N$ [13], and $C_{59}HNO$ [14]. In addition, $C_{59}HN$ can be used as a precursor to prepare other azafullerene derivatives such as the metal-doped $MC_{59}N$ (isoelectronic with M_2C_{60} solids) and $M_2C_{59}N$ (isoelectronic with M_3C_{60} superconductors, M = K^+, Na^+, Rb^+, etc.) [6,11]. As well as the single N-substitutional doping, $C_{60-m}N_m$ azafullerenes with $1 \leq m \leq 4$ have been synthesized [15,16]. Very recently, the existence of a stable $C_{48}N_{12}$ aza-fullerene has been suggested in both experiment [17] and theory [18–25]. Compared to C_{60} [3,4], $C_{48}N_{12}$ shows an enhancement of its second hyperpolarizability by about 55 % [21], making $C_{48}N_{12}$ a good candidate for optical limiting applications. It was also shown that $C_{48}N_{12}$ can be used to build diamagnetic materials because of the enhanced diamagnetic shielding factor in the carbon atom [19]. Since $C_{48}N_{12}$ is a good electron donor, it was found that putting $C_{48}N_{12}$ into a semiconducting single-walled carbon nanotube (SWNT) would form a *n*-type SWNT-based transistor [25], and a molecular rectifier formed by an acceptor $C_{48}B_{12}$ and donor $C_{48}N_{12}$ pair exhibits rectification behavior [25]. The fcc solid of $C_{48}N_{12}$ was shown to be a semiconducting material [21]. All these studies suggest potential applications of $C_{48}N_{12}$ as semiconductor components, nonlinear optical materials, and possible building blocks for photonic devices and molecular electronics. Since $C_{48}N_{12}$ has many isomers, one of our purposes in this paper is to identify physical properties to distinguish the isomer structures of $C_{48}N_{12}$ which are required for building molecular electronic devices.

A quantitative understanding of optical excitations and absorption of molecules, clusters, and nanocrystals is important in many aspects, for example, spectroscopy, photochemistry, and the design of optical materials [26–45]. The measurement, the prediction, and interpretation of the discrete excitonic spectra of these systems is a demanding and timely task. Since the first preparation of fullerenes in macroscopic amounts [46], extensive research into the electronic absorption spectra of fullerenes and doped fullerenes has been conducted [2]. Over these years, a large number of optical measurements for fullerenes in solutions, gas phase or solid state have been reported in the UV-vis region [3,7,8,11,14,47–55]. In the meantime, theoretical calculations of the electronic structure and absorption spectra of fullerenes have been performed to identify the observed absorption spectra (see detailed review in section I of Ref. [54]). To the best of our knowledge, the experimental UV-vis spectra of $C_{59}N^+$ [8], $C_{59}HN$ [11] and its derivatives including $C_{59}HNO$ [14], $(C_{59}N)_2$ [7], $C_{59}(CHPh_2)N$ [12], $C_{59}(C_6H_4CH_3)N$ [13] and $C_{59}(C_6H_4OCH_3)N$ [13] have not been assigned by *ab initio* calculations (there is one theoretical paper discussing the UV-vis spectrum of $C_{59}HN$ by using a semiempirical method [56], but the spectral assignment of experiment is not satisfactory [57]). Therefore, the second purpose for this and our following work [57] is to calculate the low-energy excitation and absorption spectra of $C_{59}N^+$, $C_{48}N_{12}$, and $C_{59}HN$ and its derivatives [57]. Our results for $C_{59}N^+$ obtained by using TD-DFT successfully characterize our measured UV-vis and transient absorption spectra of the carborane anion salt $[C_{59}N][Ag(CB_{11}H_6Cl_6)_2]$ [8]. For $C_{48}N_{12}$, it is a prediction calculation. However, once the materials of $C_{48}N_{12}$ have been prepared in sufficient quantity and purity, the measurement of its UV-vis and transient absorption spectra is straightforward. Our theoretical prediction will be helpful in assigning the absorption spectra of $C_{48}N_{12}$ measured in the future.

Absorption spectra calculations of large molecules [58] are more demanding of computer resources and computational techniques than geometry optimizations. A common computational approach uses semi-empirical quantum chemical procedures including ZINDO (Zerner Intermediate Neglect of Diatomic Differential Overlap) to predict or explain excited states of large molecules, for example, fullerenes at the level of singles configuration interaction [59]. This approach may lead to absolute errors of > 0.5 eV on peak positions [54,60]. Unfortunately, the accuracy of this approach is not good enough to allow unequivocal differentiation of molecular isomers [54,60,61]. Currently, advanced calculations of the absorption spectra of large molecules and clusters have been possible by using *ab initio* methods, for example, TD-DFT [54,58,62–65]. Since the discovery

of C_{60} [1], detailed experimental data of C_{60} absorption spectra has been reported [47–54]. This provides a good test to optimize and challenge theoretical methods for calculating dipole-allowed electronic transitions in large molecules and clusters, and to examine their accuracy. Therefore, our third purpose of this paper is to demonstrate the utilities of ZINDO, TD-HF and TD-DFT in calculating and correctly assigning the UV-vis [47,48,50–54] and transient [66] absorption spectra of C_{60}, and report the spectral features of $C_{59}N^+$, $C_{59}HN$ and its derivatives [57], and the most stable isomer of $C_{48}N_{12}$. To support our assignment of the dominant spectral features of those azafullerenes, we present a comparison of experiment and theory for C_{60}, discuss the TD-DFT method by using different exchange, correlational and hybrid functionals, and demonstrate the importance of electron correlation effects in assigning the absorption spectra of C_{60}. Such a detailed TD-DFT study and a systematic comparison between ZINDO, TD-HF and TD-DFT results have not been reported for C_{60}. We shall see that TD-DFT with non-hybrid functionals or a LSDA is good enough to predict the low-energy optical absorption spectra of azafullerenes as well as C_{60}. It should be mentioned that Bauernschmitt *et al.* [54] were the first to employ TD-DFT to calculate UV-vis allowed transitions of C_{60}, using an exchange functional of Becke [68] plus a correlation functional of Perdew [69], i.e., BP86.

Simulations of nanosystems such as InP, InAs, CdS, CdSe and Si nanocrystals [30,38,42–45] with hundreds of atoms would be out of reach by using the TD-DFT. For such systems, semi-empirical tight-binding metods have been shown to describe them well [29,32,38,41,42]. Because of the strong electron-hole interaction, a single-particle approximation cannot in general be used in confined systems for the calculation of the excitation energies [33–35]. Thus, several methods and approximations [26,27,31,38,41,42] have been developed to treat the strong electron-hole interaction of these systems. In these approaches, the calculated results depend on the quality of the used parameters and the choice of the dielectric constant model [28,29,37,38,41,42]. Recently, Frauenheim and collaborators [70] have proposed a TD DFT-based tight-binding (TD-DFT-TB) method, i.e., the extension of their self-consistent charge-density-functional tight-binding (SCC-DFTB) method [71,72] to study the optical properties of finite system within TD-DFT. This method works without any empirical parameter and can be used to study very large systems such as nanocrystals and macromolecules with hundreds of atoms and even without any symmetry. Our last purpose of this paper is to further test the performance of the TD-DFT-TB method by applying it to heterofullerenes. We find that the TD-DFT-TB method yields reasonable agreement for optical spectra with experiments and TD-DFT calculations at a highly reduced cost.

This paper is organized as follows. Section II presents our computational methods and experimental details. Section III covers a detailed study of the UV-vis and transient absorption spectra of C_{60} including a comparison of experiment (spectra in gas phase and solution) and theory (gas phase). Section IV reports our calculated low-energy excitations and optical absorption spectrum of $C_{59}N^+$ and our measured UV-vis and transient absorption spectra of the carborane anion salt $[C_{59}N][Ag(CB_{11}H_6Cl_6)_2]$. Section V predicts the low-energy excitation and optical absorption spectra of of the most stable isomer of $C_{48}N_{12}$ and discusses the isomer effect. Finally, section VI concludes this paper.

II. DETAILS OF THEORY AND EXPERIMENT

A. Computational methods

In this paper, our interest focuses on ZINDO, TD-HF and TD-DFT, which have been implemented in the Gaussian 98 program [73], and TD-DFT-TB, which has been implemented in the computing code by Frauenheim and collaborators [70]. In the following, we briefly review the those methods.

Traditional DFT [74] is a popular and efficient method for the calculation of ground-state properties of interacting many electron systems. Currently, there is a great deal of interest in extending DFT to study excited-state properties of molecules, clusters and nanocrystals [58,63–65]. There exist several extensions of the basic formalism. One such extension uses the time-dependent formalism which provides a promising way to calculate the frequency-dependent response functions, for example, polarizability. The excitation energies are characterized as the poles of the frequency-dependent response functions. Many applications of TD-DFT have been reported (see Ref. [54,58,60–65,75–78] and several reviews [79–84]). In TD-DFT, the time-dependent analogue of the exchange-correlation functional, E_{xc}, is a functional of the time-dependent electron density $\rho(\mathbf{r},t)$ (E_{xc} in DFT depends only on the stationary $\rho(\mathbf{r})$), and a reliable adiabatic local-density approximation is used (see Ref. [78] for an approximate solution to the TD-DFT response equations for finite systems). In this paper, we use the formalism [64,65] implemented in the Gaussian 98 program [73] and consider the following functionals: (i) the exchange functionals of Becke (B) [68], Perdew-Wang (PW91) [85,86] and Gill (G96) [87] as well as the modified PW91 (MPW) [88]; (ii) the correlation functionals of Lee, Yang and Parr (LYP: including both local and non-local terms) [89], Perdew

(PL: local, non-gradient correction) [90], Perdew (P86: the gradient corrections plus local correlation) [69], and Perdew and Wang (PW91: gradient-corrected correlation) [85,86]; and (iii) several hybrid functionals including Becke's three parameter hybrid functional with LYP (B3LYP) [91], P86 (B3P86), and PW91 (B3PW91), Becke's one parameter hybrid functional with LYP (B1LYP), Adamo and Barone's Becke-style one parameter functional using MPW exchange and PW91 correlation (MPW1PW91) [88]. The LSDA, which uses the Slater exchange [92] and the correlation functional of Vosko, Wilk and Nusair (VWN) [93], will also be discussed.

Before TD-DFT was developed, a common method that most people used was the TD-HF method [94,95], which is also known as the random phase approximation. This method leads to an approximate treatment of electronic excitation energies with no electron correlation effects. As shown before [79–84,96] and in this work, electron correlation must be included in any predictive theory for an accurate treatment of excited states of molecules, clusters and nanocrystals.

Another common approach is the ZINDO method [59], a semiempirical computational procedure to predict excited states of large molecules at the level of singles configuration interaction. This approach is based on an INDO Hamiltonian, and has been successfully applied to the calculation of excited state properties of a wide variety of organic and organometallic compounds [59]. For this method, we shall see that the choice of configuration numbers plays an important role in getting the excitonic energies converged in the low-energy region. As mentioned before and shown later, the accuracy of ZINDO is not good enough to assign correctly the observed UV-vis spectra of C_{60} and $C_{59}N^+$ (and $C_{59}HN$ and its derivatives [57]).

The TD-DFT-TB developed by Frauenheim and collaborators [70] follows the TD-DFT route of Casida [79,80] and uses a γ-approximation. In this approximation, the coupling matrix used in TD-DFT is treated by decomposing the transition density between different orbitals into atom-centered contributions. Because no integral evaluations are needed to be done, this scheme is numerically as efficient as the semiemprical tight-binding methods. Since a minimal basis set is used in the TD-DFT-TB, the optical properties for large systems, such as nanosystems, biological systems and polymers with hundreds of atoms, can be easily investigated. Especially, for the calculations of the lowest excited energies such as the optical gaps, we can obtain the results at a highly reduced cost since the size of the coupling matrix is drastically reduced [70].

B. Structures, basis sets and notes

For azafullerenes and C_{60}, all ground-state structures studied for calculating excitation energies were optimized using the DFT method with the hybrid B3LYP functional and a basis set 6-31G(d) with SVP (split valence plus polarisation) on carbon and nitrogen atoms. For the ground-state structure of C_{60}, this treatment results in excellent agreement between theory and experiment for ground-state physical quantities (for example, the bond lengths, angles and diameter of C_{60}, see details in Ref. [21]).

For *ab initio* methods, we use Pople-style basis sets. To examine the difference between results predicted by TD-DFT with various functionals, we use a minimum basis set STO-3G, which is qualitatively enough to show physical insights into our theoretical calculations. For accurate results, we use 3-21G to report our results for C_{60}, $C_{59}N^+$ and $C_{48}N_{12}$.

In this paper, we use the symbols, ${}^{(1)}E_i$ and ${}^{(3)}E_i$, to denote the energies of the ith singlet and triplet excited states, respectively. We compute the exciton participation contribution (EPC), P_n^v (i.e., probability P, in percentage), of an exciton pair (n, v) to a specified excited sate, where n and v represent the (HOMO-n)th occupied and (LUMO+v)th unoccupied single-electron states of a molecule. For example, (1,3) is an exciton pair made from HOMO-1 and LUMO+3 single-electron states. In addition, the optical excitonic gap E_g^{opt} is defined as the lowest energy of the dipole-allowed excitonic states in molecules, clusters and nanocrystals [38,41,58].

In addition, it should be noted that experiment probes the optical response of fullerenes subject to differing degrees of solvent perturbation in ground and excited states. For example, in the case of C_{60}, systematic studies [97] have indicated that at room temperature, solvent interactions generally cause red shifts of transitions relative to gas phase. Our calculations here refer to isolated ("gas phase") species with zero vibrational excitation.

C. Experimental details

The carborane anion salt, $[C_{59}N][Ag(CB_{11}H_6Cl_6)_2]$, was provided by the Reed group. Details about the synthesis of this material are given in their paper [8].

UV-vis-NIR absorption spectrum of the $C_{59}N^+$ salt reported in this paper was measured with a JASCO V-570DS spectrometer at room temperature. Transient triplet-triplet absorption spectra for C_{60} and the $C_{59}N^+$ salt were measured by using the third-harmonic generation (THG, 355 nm) of a Nd:YAG laser (Spectra-Physics, Quanta-Ray GCR-130, 6 ns fwhm) as an ex-

citation source. Details about the experimental procedures can be found in our recent work [55,66].

III. LOW-ENERGY EXCITATIONS AND ABSORPTION SPECTRUM OF C_{60}

A. Excitations and absorption spectra

Many experimental studies on the optical absorption of C_{60} have been performed. Here we focus on the low-energy excitations below 4.5 eV in the gas phase or solution [47–54]. Table I lists the experimental results of C_{60} in gas phase or solution [47–54]. Below 4.5 eV, there are only two dipole-allowed transitions (DATs) around 3.1 and 3.8 eV, both in the violet and UV regions. Both DAT peaks are slightly blueshifted in comparison with those of the condensed forms [98,99]. This shift is a result of a stronger intermolecular interaction [100] in the condensed state than in the gas phase. The measured energy $^{(1)}E_1$ of the first singlet for C_{60} in benzene (toluene) was 1.78 eV [66] (1.70 eV [67]). The first triplet energy $^{(3)}E_1$ of C_{60} was reported to be 1.65 eV [66], 1.56 eV [67], 1.63 eV [101] and 1.57 eV [102].

In Table I, we report the energies $^{(1)}E_1$ and $^{(3)}E_1$ as well as the energies ϵ_i and oscillator strength $f_{osc,i}$ of the ith DATs of C_{60} calculated by using ZINDO, TD-HF, TD-DFT-TB and TD-DFT methods. With a minimum basis set STO-3G, we find that the TD-DFT method with a LSDA and all kinds of non-hybrid functionals leads to similar results. The calculated $^{(3)}E_1$, $^{(1)}E_1$, ϵ_1 and ϵ_2 are only about 0.2 eV higher than the experimental values [47–54,66,101,102]. Moreover, the $^{(1)}E_1$, ϵ_1 and ϵ_2 predicted by the TD-DFT method with all kinds of hybrid functionals are about 1.0 eV higher than the experimental values [47–54], and it costs about 40-90 % (150%) more CPU than TD-DFT with non-hybrid functionals (LSDA).

The TD-DFT method can lead to more accurate excitation energies by using a larger double zeta valence-split basis set. For example, as shown in Fig.1(d)(e) and listed in Table I, the DAT energies ϵ_1 and ϵ_2 predicted by TD-LSDA/3-21G and TD-BP86/3-21G are only 0.1 eV lower than the experimental values [47–54], and the results obtained by TD-B3LYP/3-21G (see Fig.1(c) and Table I) are improved by about 50%.

With the ground-state structure of C_{60} optimized by SCC-DF-TB method, Frauenheim and collaborators [70] have shown that the single-particle approximation fails to reproduce the experimental spectrum. The reason is that the single-particle approximation cannot be used when the coupling between different electronic transition becomes important giving rise to collect effects of exciton pairs (as shown in following sections). However, these effects are correctly described within TD-DFT and within the γ-approximation used in TD-DFT-TB. As shown in Fig.1(b) and listed in Table I, the TD-DFT-TB predicts the spectral features correctly, whereas the two DAT energies are 0.4 (0.3) eV lower than experimental values (the TD-BP86/3-21G results).

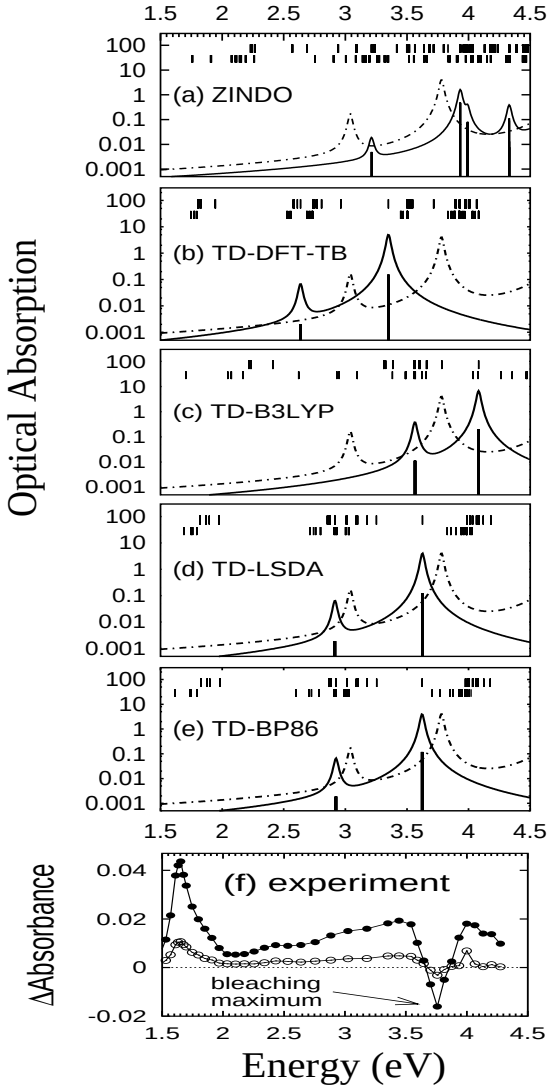

FIG. 1.: Low-energy optical absorption spectra of C_{60} calculated by using (a) ZINDO, (b) TD-DFT-TB (adapted from Ref. [70]), (c) TD-B3LYP/3-21G, (d) TD-LSDA/3-21G and (e) TD-BP86/3-21G. The vertical lines are the calculated oscillator strengths (bottom), triplet (middle) and singlet (top) energy spectra. The dot-dashed line is the experimental spectrum adapted from Ref. [50]. (f) Transient triplet-triplet absorption spectra of C_{60} in toluene observed with 355 nm laser irradiation, where filled (open) circles are spectra 5 (50) μs after a ns-laser pulse.

Table I shows that the two DATs predicted by TD-HF/3-21G occur in the UV region and the corresponding energies are blueshifted by about 2.5 eV relative to the experimental values [47–54]. Comparison with TD-DFT, TD-DFT-TB and TD-HF results reflects the importance of electron correlation effects in accurately predicting the dominant spectral features of C_{60}.

For a structureless spectral band, the oscillator strength, f_{osc}, can be obtained approximately by [50]

$$f_{osc} = 9.197 \times 10^{-9} \epsilon_{max} \Delta\nu_{1/2} \quad (1)$$

where $\Delta\nu_{1/2}$ is the frequency half-width of an assumed Gaussian-shaped band and ϵ_{max} the extinction coefficient of the absorption peak. The f_{osc} of C_{60} in gas phase can be estimated from the refractive index of n-hexane to be about 20 % smaller than that in the solution [50]. In light of this point, the oscillator strength calculated by TD-DFT and TD-DFT-TB is in good agreement with experiment, but that calculated by TD-HF is not.

It should be mentioned that the two DAT energies calculated by Bauernschmitt *et al.* [54] with TD-BP86/6-31G+s, as listed in Table I, are about 0.1 eV lower than ours calculated by TD-BP86/3-21G, and their calculated oscillator strengths f_{osc} are slightly larger than ours. In addition, our calculated DAT energies and oscillator strengths with TD-HF/3-21G are consistent with those calculated by Weiss, Ahlrichs and Häser [95] with TD-HF/6-31G+s (see Table I).

Using ZINDO, we find that the excitation energies below 4.5 eV, as reported in Table I, are converged within 0.003 to 0.03 eV as the configuration number increases from 1600 (HOMO-n, LUMO+n, n=0,1,...39) to 2500 (HOMO-n, LUMO+n, n=0,1,...49). The first two DAT energies ϵ_1 and ϵ_2 predicted by ZINDO are similar to those predicted by TD-DFT/STO-3G with a LSDA or non-hybrid functionals. In Fig.1(a), we report the absorption spectra of C_{60} calculated with 2500 configuration. In comparison with TD-DFT and TD-DFT-TB, ZINDO yields significantly different relative intensities of the oscillator strengths, and predicts two new DATs at 4.01 and 4.33 eV, which are absent in the experimental spectrum. Moreover, as shown in Table I, ZINDO with 2500 configuration predicts better spectral features than CINDO/s with 900 configurations by Braga *et al.* [103]. Thus, the calculation methods and the size of the configuration sets affect both the excitation energies and oscillator strengths of the DATs as evidenced before [50,103] and this work. It should be mentioned that the first DAT (ϵ_1) depends strongly on the carbon-carbon bond lengths and on whether equal or alternating bond lengths are used [50]. As a result, the oscillator strength f_{osc} calculated by different theoretical groups varies from 0.07 to 0.27 [50].

In Table I, we listed the calculated energies $^{(3)}E_1$ of the first triplet of C_{60}. Comparison with the calculated and measured $^{(3)}E_1$ shows that TD-DFT and TD-DFT-TB leads to more accurate results than ZINDO. It should be noted that the $^{(3)}E_1$ predicted by TD-HF is negative, i.e., this theory predicts a triplet ground state (Stratmann *et al.* [65] found similar TD-HF results for C_{70}).

The technique of measuring the transient absorption spectrum of a molecule can be used to study and characterize the triplet-triplet absorption bands. In Fig.1(f), we report the transient triplet-triplet absorption spectrum of C_{60} in toluene observed with 355 nm laser irradiation. This is in agreement with the laser flash photolysis experiment of C_{60} in bezene reported by Dimitrijević and Kamat [104]. From Fig.1(f), we find absorption maxima at 1.65, 2.43, 3.10, 3.44 and 3.98 eV and a bleaching maximum at 3.76 eV. The bleaching maximum coincides well with the UV maximum absorption at 3.73 eV. The isosbestic points, which confirm the conversion of C_{60} into its triplet excited state, are observed at 3.65 eV (340 nm) and 3.87 eV (320 nm), which are in excellent agreement with those (343 nm and 325 nm) observed by Dimitrijević and Kamat [104].

In Fig.1(a-e), we present the triplet energy spectrum calculated with TD-DFT, TD-DFT-TB and ZINDO methods. It is seen that TD-LSDA, TD-BP86 and TD-DFT-TB lead to similar triplet spectra, and the predicted triplet-triplet energy bands around 1.6 eV and 3.0 eV characterize well the transient absorption experiment. However, the triplet spectra predicted by TD-B3LYP and ZINDO are not in good agreement with our experiment.

B. Exciton pair contribution

To understand the absorption spectra predicted by TD-DFT, we have analysed the single-electron energy levels and orbital symmetries of C_{60} in its ground state. The electronic structures of C_{60} predicted by using LSDA, non-hybrid and hybrid functionals show a common feature: the HOMO and LUMO have h_u and t_{1u} symmetry, respectively.

As shown in Fig. 2, the level ordering and symmetries obtained with LSDA and non-hybrid functionals are the same by use of either STO-3G or 3-21G basis set. With the increasing of the basis size, the ordering and symmetries of occupied orbitals do not change, but the unoccupied orbitals with t_{2u} and h_g symmetry exchange the ordering (i.e., the unoccupied orbital with t_{2u} symmetry has a slightly lower energy than the unoccupied orbital with h_g symmetry).

For hybrid functionals, the computed orbital ordering and symmetries for the ground-state C_{60} are also the same by use of either STO-3G or 3-21G basis set. For

STO-3G basis set, in comparison with the level diagram predicted by using LSDA or non-hybrid functionals, the ordering and symmetries of unoccupied orbitals do not change, but those for occupied orbitals with h_g and g_g symmetry exchange (i.e., as shown in Fig. 2, the occupied orbital with g_g symmetry has a slightly lower energy that that with h_g symmetry). However, for 3-21G basis set, all functionals predict the same level ordering and symmetries for both occupied and unoccupied orbitals.

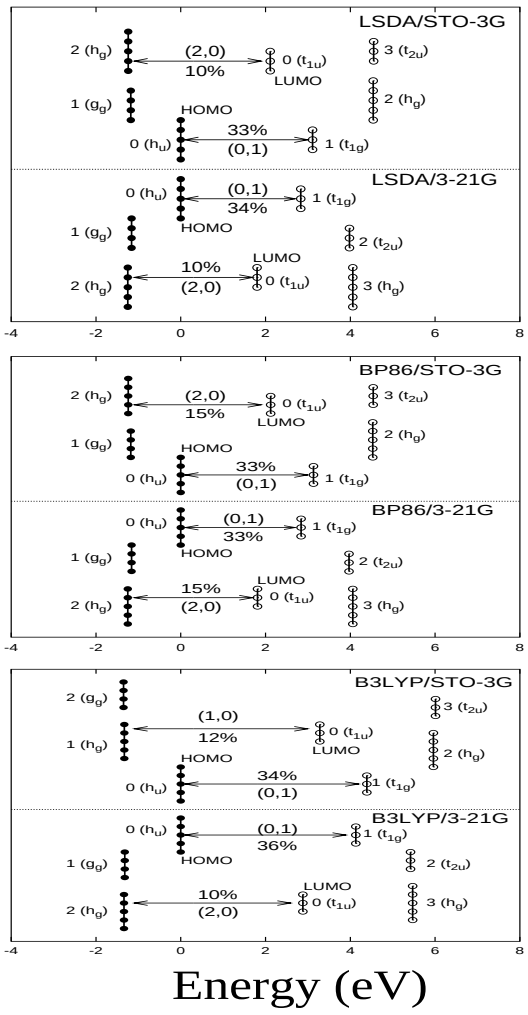

FIG. 2.: Single-electron energy levels (LUMO+v with v=0,1,2,3, and HOMO-n with n=0,1,2), orbital symmetries and degeneracies of C_{60} in the ground state calculated by LSDA, BP86 and B3LYP with STO-3G and 3-21G basis set, where all energies are shifted with reference to the HOMO energy and filled (open) circles denote occupied (unoccupied) orbitals. The exciton pair contributions P_n^v of exciton pairs (n, v) to the first dipole-allowed singlet are shown as an example.

To see the collective effects of exciton pairs, Table II lists the EPCs P_n^v of exciton pairs (n, v) to the first singlet state ($^{(1)}E_1$) and the first two DAT states (ϵ_1 and ϵ_2) predicted by TD-DFT. No matter which functionals we use, we find a common feature from the calculated EPCs: (1) $^{(1)}E_1$ comes mainly from the contribution of the exciton pair made by HOMO and LUMO; (2) ϵ_1 is mainly from the EPCs of two exciton pairs, one made by the HOMO and the unoccupied orbital with t_{1g} symmetry, and one made by the LUMO and the occupied orbital with h_g symmetry; (3) ϵ_2 originates from the EPCs of three exciton pairs, one made by the LUMO and the occupied orbital with h_g symmetry and two made by HOMO and the unoccupied orbitals with t_{1g} and h_g symmetry. As a result, the first singlet is fourfold-degenerate and dipole-forbidden, e the two DATs are triply-degenerate and the collective effects of exciton pairs become important for the two DATs.

In Table III, we list the EPCs P_n^v to the triplet states in the first two triplet energy bands predicted by TD-BP86/3-21G shown in Fig.1(e). We find that the first band comes from the exciton pair formed by t_{1u} LUMO and h_u HOMO, while the second band from three kinds of exciton pairs made by HOMO-2 (h_g)/LUMO, HOMO/LUMO+1 (t_{1g}) and HOMO-1 (g_g)/LUMO.

It should be mentioned that the EPCs to the first two DAT states predicted by ZINDO are different from the common features obtained from TD-DFT. The first DAT is mainly from three exciton pairs made by the h_u HOMO and the unoccupied orbitals with t_{1g}, t_{2u} and h_g symmetry. The second DAT comes mainly from two exciton pairs made by the h_u HOMO and the unoccupied orbitals with t_{1g} and t_{2g} symmetry. In addition, the EPCs to the first singlet and the first two DATs predicted by TD-HF are simlar to those obtained by TD-DFT.

IV. LOW-ENERGY EXCITATION AND ABSORPTION SPECTRA OF $C_{59}N^+$

A. Theory

Fullerene's symmetry plays an important role on the excitation and optical absorption spectra of fullerenes since the symmetry determines the optical activity [2,3]. The substitutional doping of one or several dopants into C_{60} obviously lowers its I_h symmetry, and correspondingly modifies the symmetries of molecular orbitals [2]. In this section, we take $C_{59}N^+$ [7,8] as an example to study the symmetry effect.

Although it is an isoelectronic analogue to C_{60}, $C_{59}N^+$ has C_s symmetry. Thus, from the energy diagram of the ground-state $C_{59}N^+$ shown in Fig.3, we find that the degeneracy of the original levels of the

ground-state C_{60} presented in Fig.2 (for example, the fivefold degeneracy of HOMO and the threefold degeneracy of LUMO) is completely removed and the orbital symmetry is correspondingly changed to either $a^{'}$ or $a^{''}$ symmetry. Therefore, as reported in Fig.4 and Fig.5, $C_{59}N^{+}$ exhibit richer features in the triplet, singlet and optical absorption spectra than C_{60}. For example, the narrow singlet and triplet bands predicted for C_{60} are completely split and expanded.

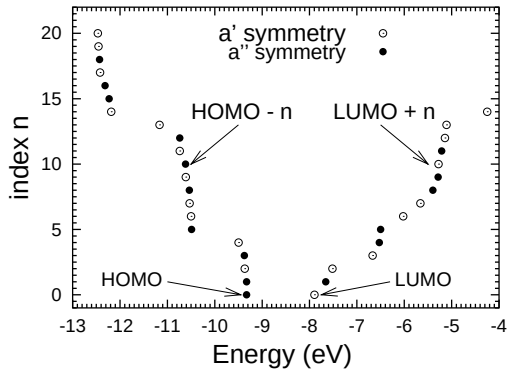

FIG. 3.: Single-electron energy levels (LUMO+n and HOMO-n) of $C_{59}N^{+}$ in its ground state calculated by BP86/3-21G. Open (filled) circles denote $a^{'}$ ($a^{''}$) symmetries of molecular orbitals.

As discussed in section III, the LUMO (HOMO) of C_{60} has t_{1u} (h_u) symmetry and thus the first singlet of C_{60} is dipole-forbidden. In contrast, the LUMO (HOMO) of $C_{59}N^{+}$ has $a^{'}$ ($a^{''}$) symmetry. As reported in Table IV for TD-BP86/3-21G, the first singlet of $C_{59}N^{+}$ with an energy of 1.49 eV is dipole-allowed and comes mainly from the (1,0) and (0,0) exciton pairs which originate from the C_{60} HOMO and LUMO. Thus, the optical gap of $C_{59}N^{+}$ is redshifted by 1.44 eV relative to that of C_{60}.

In the visible region reported in Fig.4(a), the absorption spectrum of $C_{59}N^{+}$ calculated by TD-BP86/3-21G shows three relatively strong dipole-allowed transitions at 2.66, 2.72 and 2.79 eV. As listed in Table IV, they are mainly from the EPCs of (6,0), (7,0) and (10,0) exciton pairs, respectively. The dipole-allowed transition at 2.79 eV is similar to the first dipole-allowed transition (at 2.92 eV) predicted for C_{60} since the exciton pairs (see Table IV) contributing to this transition originate from the h_u HOMO, h_g HOMO+2, t_{1u} LUMO and t_{1g} LUMO+1 of C_{60}. Moreover, we find several weaker dipole-allowed transitions occuring at 1.52, 1.55, 1.68, 1.95 and 2.09 eV. As listed in Table IV, they are mainly due to the EPCs of (3,0), (2,0), (4,0), (2,2) and (4,2) exciton pairs, respectively, which actually originate from the h_u HOMO and t_{1u} LUMO of C_{60}, and little collective effects of other exciton pairs. In the UV region, several strong dipole-allowed transitions occur at 3.51, 3.59, 3.68 and 3.69 eV. The EPCs to those transition states are listed in Table IV. It shows strong collective effects of exciton pairs for those transitions. The transition at 3.59 eV is very similar to the second dipole-allowed singlet state (ϵ_2 = 3.62 eV) of C_{60} since the main exciton pair to this transition originate from the t_{1u} LUMO and h_g HOMO+2 of C_{60}.

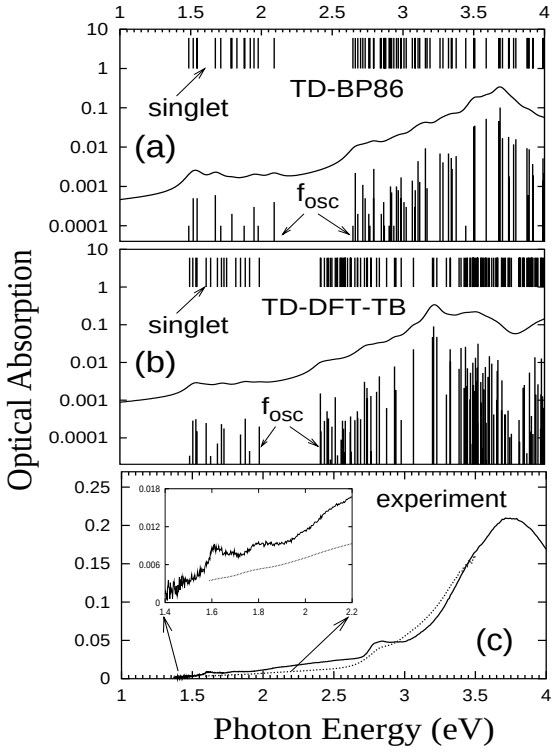

FIG. 4.: (a) Optical absorption spectra of $C_{59}N^{+}$ calculated by using BP86/3-21G, where the vertical lines are the calculated oscillator strengths f_{osc} (bottom) and singlet energies (top). (b) UV-vis spectrum of $C_{59}N^{+}$ (concentration: 10μM) in toluene. The dotted line is the visible spectra of $C_{59}N^{+}$ (concentration: 0.00138 M) in o-dichlorobenzene adapted from Ref. [8].

In Fig. 5, we also report the triplet energy spectrum of $C_{59}N^{+}$ calculated by TD-BP86/3-21G. It is distinguished by two triplet bands in the visible region. In Table IV, we list P_n^v to the first triplet band, which contains $^{(3)}E_i$ ($i = 1, 2, ..., 15$). Actually, this originates from the first triplet band of C_{60}, i.e., they are mainly from the exciton pairs made by the occupied and unoccupied orbitals splitted from the LUMO and HOMO of C_{60} due to the removal of degeneracy. For example, the first triplet of $C_{59}N^{+}$ comes mainly from the (0,0), (1,0) and (3,0) exciton pairs which originate from the C_{60} LUMO and HOMO, and has an energy of 1.35 eV

that is redshifted by 0.27 eV relative to the calculated $^{(3)}E_1$ of C_{60}.

In comparison with TD-DFT and TD-DFT-TB results shown in Fig. 4 and Fig. 5, we find that the TD-DFT-TB predicts similar spectral features for $C_{59}N^+$. Especially, below 2.2 eV, the calculated energies for the lowest singlet /triplet states are in good agreement with TD-DFT. In the blue and violet region (2.5 to 3.1 eV), the sinlget/triplet excitation energies are redshifted by about 0.2 eV in comparison with the TD-DFT calculations. In the UV region, the redshift is about 0.5 eV. Thus, TD-DFT-TB yields good results for the lowest singlet/triplet states.

B. Experiment

As shown before [11] and in our following serial work [57], the spectroscopic properties of heterofullerenes can be used as references for the characterization of their functionalized complexes. Here we demonstrate this point for $C_{59}N^+$.

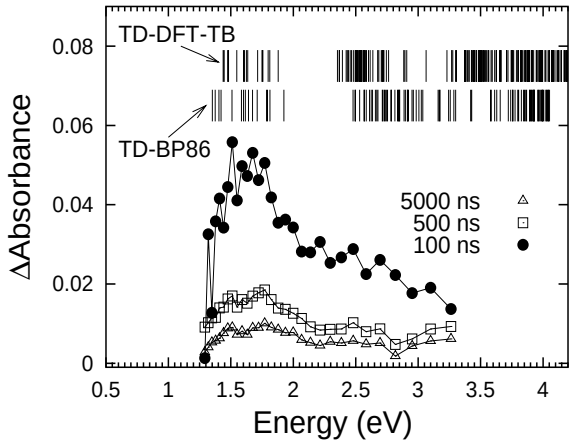

FIG. 5.: Transient triplet-triplet absorption spectra of $C_{59}N^+$ in toluene (the concentration condition was 10 mM) observed by 355 nm laser irradiation. Filled circles, open squares and triangles are spectra 100, 500 and 5000 ns after a ns-laser pulse, respectively. Vertical lines are the $^{(3)}E_i$ for $C_{59}N^+$ calculated by TD-BP86/3-21G (middle) and TD-DFT-TB (top).

Recently, Reed and coworkers [8] have reported that the monomeric cation $C_{59}N^+$ can be isolated as a carborane anion salt, i.e, $[C_{59}N][Ag(CB_{11}H_6Cl_6)_2]$. They measured the visible spectrum of this salt in *o*-dichlorobenzene (see the dotted line in Fig.4(c)). Their spectrum is quite featureless, showing only a narrow shoulder between 2.8 and 2.9 eV. Our measured UV-vis spectrum for this salt in toluene, shown in Fig.4(c), reproduces the shoulder, but a bit broader than theirs. Our calculated UV-vis spectrum characterizes well this shoulder. Especially, our measured absorption spectrum in the visible region shows two absorption maxima at 1.61 and 1.80 eV, respectively (note: a much weaker absorption at 1.8 eV was actually observed in the visible spectrum of Reed's group), which are in good agreement with our calculations (1.49 and 1.68 eV). The measured redshift of the optical gap (E_{og}=1.61 eV) of $C_{59}N^+$ relative to the optical gap (E_{og}=3.05 eV) [51] of C_{60} is 1.44 eV, in excellent agreement with the redshift predicted by TD-BP86/3-21G. In the UV region, the measured maximum absorption at 3.69 eV is in excellent agreement with our predicted maximum absorption at 3.69 eV.

We irradiate a toluene solution of this salt with a nanosecond laser light at 355 nm. The results are shown in Fig.5. We find that the irradiation generated a transient triplet-triplet absorption band centered at 1.60 eV. This band is much broader than that of C_{60} shown in Fig.1(e) and was observed in the microsecond range. The lifetime of the triplet state was estimated to be 0.3 μs, quicker than that of C_{60} (40μs [66] and 55μs [67]) and $C_{59}HN$ (5μs [55]). As shown in Fig.5, our calculated triplet energies in the first triplet band characterize well the transient triplet-triplet absorption band. The measured $^{(3)}E_1$-redshift of $C_{59}N^+$ relative to C_{60} is 0.30 eV, in excellent agreement with the calculated redshift (0.27 eV).

Therefore, our above theoretical and experimental results have demonstrated that the spectroscopic properties of $C_{59}N^+$ can be used as a reference for the characterization of functionalized complexes, such as the carborane anion salts.

V. LOW-ENERGY EXCITATION AND ABSORPTION SPECTRA OF $C_{48}N_{12}$

As shown in section IV, the substitutional doping of one nitrogen atom into C_{60} lowers the symmetry of I_h to a C_s symmetry and produces the rich absorption spectra of $C_{59}N^+$. As the substitutional number of nitrogen atoms increases up to 12, the existence of two stable $C_{48}N_{12}$ isomers was suggested (note: the most stable isomer I [20] is about 13.1 kcal/mol lower in energy than the second stable isomer II [17]). Both isomers have S_6 symmetry, which is higher (lower) than that of $C_{59}N^+$ (C_{60}), and they are isoelectronic with C_{60}^{-12} (i.e., replacing 12 carbon atoms by 12 nitrogen atoms results in a complete filling of 12 electrons into the t_{1u} LUMO and t_{1g} LUMO+1 (see Fig.2) of C_{60}). As a result, the degeneracy of orbitals in C_{60} is partially removed. As shown in Fig.6, the molecular orbitals in the ground-state $C_{48}N_{12}$ are either doubly-degenerate or non-degenerate. Thus, $C_{48}N_{12}$ would exhibit richer

spectral features than C_{60}, but less than $C_{59}N^+$.

First, we report the low-energy excitation and absorption spectra of the most stable isomer I [20] of $C_{48}N_{12}$ calculated by TD-BP86/3-21G. The results are shown in Fig.7(a) and listed in Table V. We find doubly-degenerate excited states for this isomer. The calculated absorption spectrum shows several absorption maxima at 2.12, 2.35, 2.80 and 3.41 eV in the yellow, green, violet regions, respectively, and at 3.64, 3.95, and 4.10 eV in the UV region. The main EPCs for those maximum absorptions are listed in Table V. The absorptions in the UV region show strong collective effects of exciton pairs. The first singlet/triplet states are doubly-degenerate and come from the (0,0) exciton pair. We find that the optical gap (E_g^{opt} = 1.698 eV) and the first triplet energy ($^{(3)}E_1$=1.547 eV) for the isomer I are blueshifted by about 0.2 eV relative to those of $C_{59}N^+$, but are redshifted by 1.22, 0.07 eV, respectively, relative to those of C_{60}. In Fig. 7(a), we show the corresponding triplet energy spectrum, which is distinguished by five bands in the visible region. The EPCs to the first few bands are listed in Table V. We find that the 3rd and 6th triplets involve strong collective effects of exciton pairs, while others are mainly due to the (0,0), (0,1), (0,2), (1,1), (1,2) or (2,0) exciton pair.

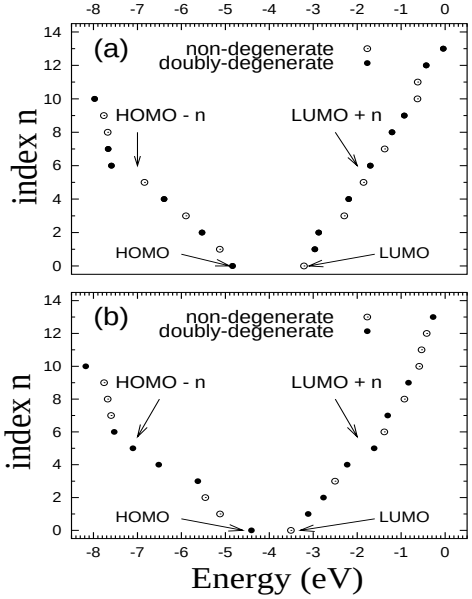

FIG. 6.: Single-electron energy levels (LUMO+n and HOMO-n) of (a) the isomer I and (b) the isomer II for $C_{48}N_{12}$ in the ground state calculated by BP86/3-21G.

The synthesis of $C_{48}N_{12}$ fullerene-analog [17] opens up the opportunity of examining the stabilities and energetics of isomers [20] of $C_{48}N_{12}$ with nitrogen-nitrogen bonded congregates [23]. Here it would be interesting to study the isomer effects on the optical absorption spectrum of $C_{48}N_{12}$. We calculated the excitation and optical absorption spectrum of the stable isomer II [17] of $C_{48}N_{12}$ by using TD-BP86/3-21G. The results are presented in Fig. 8(a) and listed in Table VI. Compared to the most stable isomer I, the isomer II shows a much stronger absorption at the first singlet state with an energy of 1.00 eV, which is redshifted by 0.70 eV relative to that of the isomer I. As shown in Fig. 8(a), the two strong dipole-allowed transitions at 2.12 and 2.35 eV predicted for the most stable isomer I are redshifted by about 0.3 eV. This result shows that the isomers of $C_{48}N_{12}$ can be distinguished from their UV/visible spectra, which characterize the detailed isomer structures that are needed, for example, in designing the molecular electronic devices (molecular rectifiers, carbon nanotube-based p-n junctions) proposed by us [25].

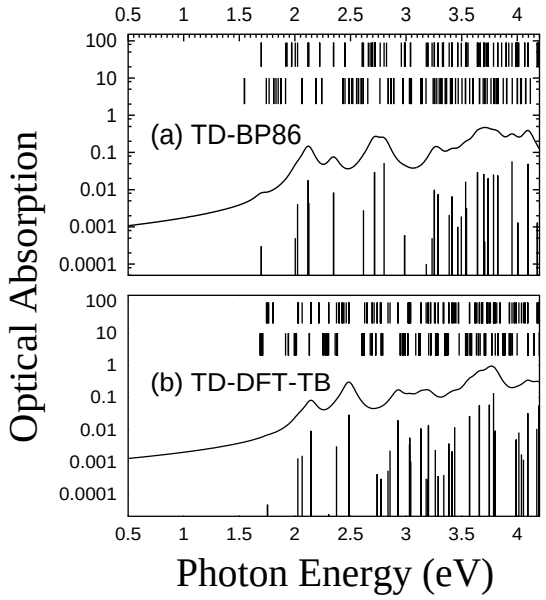

FIG. 7.: Optical absorption spectra of the stable isomer I of $C_{48}N_{12}$ calculated by (a) TD-BP86/3-21G and (b) TD-DFT-TB. The vertical lines are the calculated oscillator strengths f_{osc} (bottom), triplet (middle) and singlet (top) energy spectra.

As discussed before, the bleaching maximum and the isosbestic points characterize the transient absorption spectrum. This would provide a convenient way to spectrally distinguish the excited isomers of $C_{48}N_{12}$, especially when they are generated together in a system containing all kinds of isomers. From Fig. 8(a), we find that the triplet spectrum of the isomer II is also different from that of the isomer I: (1) there are more than five triplet energy bands in the visible region; (2) the first triplet energy is redshifted by 0.74 eV; and (3) the second triplet-triplet band is redshifted by about

0.60 eV. Thus, transient triplet-triplet absorption experiment would also help us distinguish the $C_{48}N_{12}$ isomers which are needed for molecular electronics.

For both isomers, the TD-DFT-TB results are reported in Fig. 7(b) and Fig. 8(b). In comparison with the TD-DFT results, the TD-DFT-TB predicts similar spectral features for both isomers. For the most stable isomer, we find that the calculated excitation energies in the visible region are slightly blueshifted and those in the UV region are redshifted by about 0.3 eV relative to those obtained by TD-DFT. However, for the isomer II, the calculated excitation energies below 2.5 eV are blueshifted by about 0.5 eV, whereas those between 2.5 and 4.0 eV are in good agreement with those predicted by TD-DFT. Thus, TD-DFT-TB yields reasonable results for the prediction of the excitation energies for $C_{48}N_{12}$.

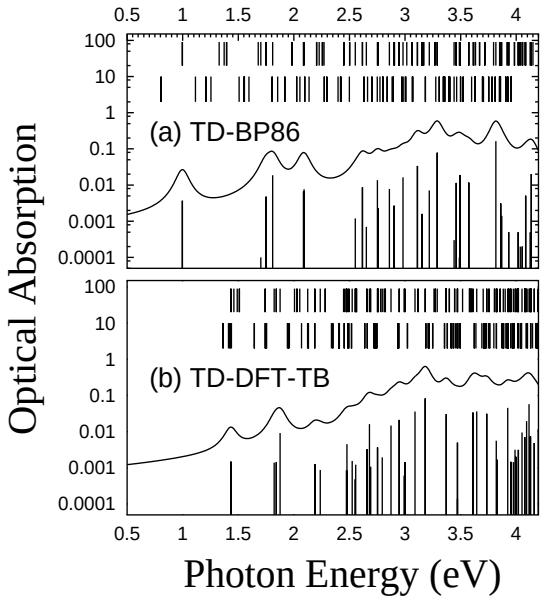

FIG. 8.: Optical absorption spectra of the stable isomer II of $C_{48}N_{12}$ calculated by (a) TD-BP86/3-21G and (b) TD-DFT-TB. The vertical lines are the calculated oscillator strengths f_{osc} (bottom), triplet (middle) and singlet (top) energy spectra.

VI. CONCLUSIONS AND REMARKS

In summary, we have performed semiempirical and *ab initio* calculations of the low-energy excitations and absorption spectra of C_{60} by using ZINDO, TD-HF, TD-DFT and TD-DFT-TB methods. A detailed comparison of experiment and theory for the optical excitonic gap, excitation and absorption spectra of C_{60} is presented. With a minimum basis set STO-3G, it is found that TD-DFT with a non-hybrid functional or a LSDA leads to more accurate excitation energies than that with a hybrid functional. In comparison with TD-HF, the TD-DFT results reveal the importance of electronic-correlation effects in assigning accurately the spectral features of C_{60}. In TD-DFT, increasing the basis set size generally leads to more accurate excitation energies. The level of agreement between theory and experiment for C_{60} supports the accuracy of similar calculations for $C_{59}N^+$ and $C_{48}N_{12}$. Our calculated absorption spectrum of $C_{59}N^+$ successfully characterizes the visible spectrum of the carborane anion salt $[C_{59}N][Ag(CB_{11}H_6Cl_6)_2]$ measured by Reed's [8] and our present experiments. We also predict rich structures of excitations and absorption spectrum of $C_{48}N_{12}$. We point out that the characterization of the UV-vis and transient absorption spectra of $C_{48}N_{12}$ isomers will distinguish the isomer structures required for applications in molecular electronics. The optical spectra of $C_{59}N^+$ and $C_{48}N_{12}$ as well as C_{60} predicted by TD-DFT-TB are in reasonable agreement with TD-DFT calculations at a highly reduced cost.

Since C_{60}, $C_{59}N^+$ and $C_{48}N_{12}$ differ in their optical gaps ranging from the violet to the red region, they may be used as single-molecule fluorescent probes [105] for applications in polymer science, biology and medicine [106,107], for example, labeling DNA and RNA, lighting up polymers, photodynamic therapy, detection and identification of fullerene-based drugs.

As discussed in this paper and previous work [70], the TD-DFT-TB method works well for π electron systems. On the other hand, this method uses a minimum basis set and does not employ any empirical parameter. Thus, the TD-DFT-TB is useful to study the optical properties of (hetero)fullerenes, functionalized (hetero)fullerenes with organic molecules, (hetero)fullerene clusters and carbon nanotubes, which have potential applications in optoelectronics [2–4], and to predict efficiently the optical gaps of large nanocrystals such as CdS and CdSe, for which the TD-DFT cannot reach.

ACKNOWLEDGMENT

RHX would like to thank the HPCVL at Queen's University for the use of its parallel supercomputing facilities, and Dr. Carlos Gonzalez, Professor Christopher A. Reed, and Dr. Javier Aizpurua for valuable discussions and comments. We thank Professor Hisanori Shinohara, Dr. Nikos Tagmatarchis, Professor Tapas Kar, and Dr. Zhongfang Chen for useful discussions. G.S. thanks NCI-Frederick, NIH for a Visiting Fellow Award. VHS gratefully acknowledges the support from the Natural Science and Engineering Research Council of Canada. MRM work was performed under the

auspices of the U.S. Department of Energy by the Lawrence Livermore National Laboratory (LLNL) under contract number W-7405-Eng-48. DH acknowledges CMS/MRI summer internship at LLNL. We thank Professor Christopher A. Reed and Dr. Kee-Chan Kim for providing the visible spectrum and the gift sample of the carborane anion salt $[C_{59}N][Ag(CB_{11}H_6Cl_6)_2]$. We thank Dr. Zhongfang Chen for sending us the coordinates of one isomer of $C_{48}N_{12}$.

[1] H. W. Kroto, J. R. Heath, S. C. O'Brien, R. F. Curl, and R. E. Smalley, Nature (London) **318**, 162 (1985).

[2] M. S. Dresselhaus, G. Dresselhaus, and P. C. Eklund, *Science of Fullerenes and Carbon Nanotubes* (Academic Press, New York, 1996).

[3] R. H. Xie, "Nonlinear Optical Properties of Fullerenes and Carbon Nanotubes", in: *Handbook of Advanced Electronic and Photonic Materials and Devices, Vol. 9: Nonlinear Optical Materials*, H. S. Nalwa (Ed.) (Academic Press, New York, 2000), pp.267-307.

[4] R. H. Xie, Q. Rao, and L. Jensen, "Nonlinear Optics of Fullerenes and Carbon Nanotubes", in: *Encyclopedia of Nanoscience and Nanotechnology* , H.S. Nalwa (Ed.) (American Scientific Publisher, California, 2003).

[5] E. Osawa (ed.), *Perspectives of Fullerene Nanotechnology* (Kluwer, New York, 2002).

[6] W. Andreoni, A. Curioni, K. Holczer, K. Prassides, M. Keshavarz-K, J.C. Hummelen, and F. Wudl, J. Am. Chem. Soc. **118**, 11335 (1996).

[7] J. C. Hummelen, B. Knight, J. Pavlovich, R. Gonzalez, and F. Wudl, Science **269**, 1554 (1995).

[8] K. C. Kim, F. Hauke, A. Hirsch, P. D. W. Boyd, E. Carter, R. S. Armstrong, P. A. Lay, and C. A. Reed, J. Am. Chem. Soc. **125**, 4024 (2003).

[9] J. C. Hummelen, C. Beilavia-Lund, and F. Wudl, Top. Curr. Chem. **199**, 93 (1999).

[10] A. Hirsch and B. Nuber, Acc. Chem. Res. **32**, 795 (1999).

[11] M. Keshavarz-K, R. González, R. G. Hicks, G. Srdanov, V. I. Srdanov, T. G. Collins, J. C. Hummelen, C. Bellavia-Lund, J. Pavlovich, F. Wudl, and K. Holczer, Nature (London) **383**, 147 (1996).

[12] C. Bellavia-Lund, R. González, J.C. Hummelen, R. G. Hicks, A. Sastre, and F. Wudl, J. Am. Chem. Soc. **119**, 2946 (1997).

[13] B. Nuber and A. Hirsch, Chem. Commun., 405 (1998).

[14] N. Tagmatarchis, H. Shinohara, T. Pichler, M. Krause, and H. Kuzmany, J. Chem. Soc., Perkin Trans. 2, 2361 (2000).

[15] T. Pradeep, V. Vijayakrishnan, A. K. Santra, and C. N. R. Rao, J. Phys. Chem. **95**, 10564 (1991)

[16] R. Yu, M. Zhan, D. Cheng, S. Yang, Z. Liu, and L. Zheng, J. Phys. Chem. **99**, 1818 (1995).

[17] L. Hultman, S. Stafström, Z. Czigány, J. Neidhardt, N. Hellgren, I. F. Brunell, K. Suenaga, and C. Cooliex, Phys. Rev. Lett. **87**, 225503 (2001).

[18] S. Stafström, L. Hultman, and N. Hellgren, Chem. Phys. Lett. **340**, 227 (2001).

[19] R. H. Xie, G. W. Bryant, and V. H. Smith, Jr., Chem. Phys. Lett. **368**, 486 (2003).

[20] M. R. Manaa, D. W. Sprehn, and H. A. Ichord, J. Am. Chem. Soc. **124**, 13990 (2002).

[21] R. H. Xie, G. W. Bryant, L. Jensen, J. Zhao, and V. H. Smith, Jr., J. Chem. Phys. **118**, 8621 (2003).

[22] R. H. Xie, G. W. Bryant, and V. H. Smith, Jr., Phys. Rev. B **67**, 155404 (2003).

[23] M. R. Manaa, D. W. Sprehn, and H. A. Ichord, Chem. Phys. Lett. **374**, 405 (2003).

[24] B. Schimmelpfennig, H. Agren, and S. Csillag, Synthetic Metals **132**, 265 (2003).

[25] R. H. Xie, G. W. Bryant, J. Zhao, V. H. Smith, Jr., A. Di Carlo, and A. Pecchia, Phys. Rev. Lett. **90**, 206602 (2003).

[26] J. Rogan and J.E. Inglesfield, J. Phys. C **14**, 3585 (1981).

[27] G. Allan, C. Delerue, and M. Lannoo, Phys. Rev. B **48**, 7951 (1993).

[28] C. Delerue, M. Lannoo, and G. Allan, Phys. Rev. Lett. **76**, 3038 (1996).

[29] N. A. Hill and K. B. Whaley, Phys. Rev. Lett. **76**, 3039 (1996).

[30] A. P. Alivisatos, Science **271**, 933 (1996).

[31] K. Leung and K. B. Whaley, Phys. Rev. B **56**, 7455 (1997).

[32] C. M. Goringe, D. R. Bowler, and E. Hernandez, Rep. Prog. Phys. **60**, 1447 (1997).

[33] S. Ogüt, J. R. Chelikowsky, and S. G. Louie, Phys. Rev. Lett. **79**, 1770 (1997).

[34] R. W. Godby and I. D. White, Phys. Rev. Lett. **80**, 3161 (1998).

[35] A. Franceschetti, L. W. Wang, and A. Zunger, Phys. Rev. Lett. **83**, 1269 (1999).

[36] I. Vasiliev, S. Ogüt, and J. R. Chelikowsky, Phys. Rev. Lett. **82**, 1919 (1999).

[37] C. Delerue, M. Lannoo, and G. Allan, Phys. Rev. Lett. **84**, 2457 (2000).

[38] S. Lee, L. Jönsson, J. W. Wilkins, G. W. Bryant, and G. Klimeck, Phys. Rev. B **63**, 195318 (2001).

[39] I. Vasiliev, S. Ogüt, and J. R. Chelikowsky, Phys. Rev. Lett. **86**, 1813 (2001).

[40] I. Vasiliev, S. Ogüt, and J. R. Chelikowsky, Phys. Rev. B **65**, 115416 (2002).

[41] R. H. Xie, G. W. Bryant, S. Lee, and W. Jaskólski, Phys. Rev. B **62**, 235306 (2002).

[42] G. W. Bryant and W. Jaskólski, Phys. Rev. B **67**, 205320 (2003).

[43] S. Ogüt, R. Burdick, Y. Saad, and J. R. Chelikowsky, Phys. Rev. Lett. **90**, 127401 (2003).

[44] L. W. Wang, M. Califano, A. Zunger, and A. Franceschetti, Phys. Rev. Lett. **91**, 056404 (2003).

[45] M. C. Troparevsky, L. Kronik, and J. R. Chelikowsky, J. Chem. Phys. **119**, 2284 (2003)
[46] W. Krätschmer, L. D. Lamb, K. Fostiropoulos, and D. R. Huffman, Nature (London) **347**, 354 (1990).
[47] H. Ajie, M. M. Alvarez, S. J. Anz, R. D. Beck, F. Diederich, K. Fostiropoulos, D. R. Huffman, W. Krätschmer, Y. Rubin, K.E. Schriver, D. Sensharma, and R. L. Whetten, J. Phys. Chem. **94**, 8630 (1990).
[48] J. P. Hare, H. W. Kroto, and R. Taylor, Chem. Phys. Lett. **177**, 394 (1991).
[49] Z. Gasyna, P. N. Schatz, J. P. Hare, T. J. Dennis, H. W. Kroto, R. Taylor, and D. R. M. Walton, Chem. Phys. Lett. **183**, 283 (1991).
[50] S. Leach, M. Vervloet, A. Despres, E. Breheret, J. P. Hare, T. J. Dennis, H. W. Kroto, R. Taylor, and D. R. M. Walton, Chem. Phys. **160**, 451 (1992).
[51] R. V. Bensasson, E. Bienvenue, M. Dellinger, S. Leach, and P. Seta, J. Phys. Chem. **98**, 3492 (1994).
[52] P. F. Coheur, M. Carleer, and R. Colin, J. Phys. B **29**, 4987 (1996).
[53] J. Hora, P. Panek, K. Navratil, B. Handlirova, and J. Humlicek, Phys. Rev. B **54**, 5106 (1996).
[54] R. Bauernschmitt, R. Ahlrichs, F. H. Hennrich, and M. M. Kappes, J. Am. Chem. Soc. **120**, 5052 (1998).
[55] N. Tagmatarchis, H. Shinohara, M. Fujitsuka, and O. Ito, J. Org. Chem. **66**, 8026 (2001).
[56] A. M. Ren, J. K. Feng, W. Li, X. Y. Sun, and Z. R. Li, Acta Chimica Sinica **57**, 541 (1999).
[57] R. H. Xie, G. W. Bryant, G. Sun, M. C. Nicklaus, N. Tagmatarchis, H. Shinohara, Y. Araki, O. Ito, and V. H. Smith, Jr., to be submitted.
[58] I. Vasiliev, S. Ogüt, and J. R. Chelikowsky, Phys. Rev. B **65**, 115416 (2002); M. C. Troparevsky, L. Kronik, and J. R. Chelikowsky, Phys. Rev. B **65**, 033311 (2001).
[59] M. C. Zerner, "Semiempirical Molecular Orbital Methods", in: *Reviews in Computational Chemistry II*, edited by K. B. Lipkowitz and D.B. Boyd (VCH Publishers Inc., 1991), Chap.8, pp.313-366.
[60] M. Benz, M. Fanti, P. Fowler, D. Fuchs, M. Kappes, C. Lehner, R. Michel, G. Orlandi, and F. Zerbetto, J. Phys. Chem. **100**, 13399 (1996).
[61] R. Bendale and M. Zerner, J. Phys. Chem. **99**, 13830 (1995).
[62] E. Runge and E.K.U. Gross, Phys. Rev. Lett. **52**, 997 (1984).
[63] R. Bauernschmitt and R. Ahlrichs, Chem. Phys. Lett. **256**, 454 (1996).
[64] M. E. Casida, C. Jamorski, K. C. Casida, and D. R. Salahub, J. Chem. Phys. **108**, 4439 (1998).
[65] R. E. Stratmann, G.E. Scuseria, and M.J. Frisch, J. Chem. Phys. **109**, 8218 (1998).
[66] M. Fujitsuka, O. Ito, Y. Maeda, M. Kako, T. Wakahara, and T. Akasaka, Phys. Chem. Chem. Phys. **1**, 3527 (1999).
[67] M. Fujitsuka, C. Luo, O. Ito, Y. Murata, and K. Komatsu, J. Phys. Chem. A **103**, 7155 (1999).
[68] A. D. Becke, Phys. Rev. A **38**, 3098 (1988).
[69] J. P. Perdew, Phys. Rev. B **33**, 8822 (1986).
[70] T. A. Niehaus, S. Suhai, F. D. Sala, P. Lugli, M. Elstner, G. Seifert, and Th. Frauenheim, Phys. Rev. B **63**, 085108 (2001).
[71] M. Elstner, D. Porezag, G. Jungnickel, J. Elsner, M. Haugk, Th. Frauenheim, S. Suhai, and G. Seifert, Phys. Rev. B **58**, 7260 (1998).
[72] M. Elstner, D. Porezag, G. Jungnickel, Th. Frauenheim, S. Suhai, and G. Seifert, in: *Tight Binding Approach to Computational Materials Science*, P. Turchi, A. Gonis, and A. Colombo (eds.), MRS Symp. Proc. No. 491 (Materials Research Society, Pittsburgh, 1998), p. 131.
[73] Gaussian 98, Revision A.9, M. J. Frisch *et al.*, Gaussian, Inc., Pittsburgh PA, 1998. Use of this software does not constitute an endorsement or certification by NIST.
[74] W. Kohn and L. J. Sham, Phys. Rev. **140**, A1133 (1965).
[75] S. J. A. van Gisbergen, J. G. Snijders, and E. J. Baerends, J. Chem. Phys. **103**, 9347 (1995).
[76] C. Jamorski, M. E. Casida, and D. R. Salahub, J. Chem. Phys. **104**, 5134 (1996).
[77] M. Petersilka, U. J. Gossmann, and E. K. U. Gross, Phys. Rev. Lett. **76**, 1212 (1996).
[78] H. Appel, E. K. U. Gross, and K. Burke, Phys. Rev. Lett. **90**, 043005 (2003).
[79] M. E. Casida, in: *Recent Advances in Density Functional Methods*, Vol.1, edited by D. P. Chong (World Scientific, Singapore, 1995).
[80] M. E. Casida, in: *Recent Developments and Applications of Modern Density Functional Theory, Theoretical and Computational Chemistry*, Vol.4, edited by J.M. Seminario (Elsevier, Amsterdam, 1996).
[81] T. L. Beck, Rev. Mod. Phys. **72**, 1041 (2000).
[82] F. Calvayrac, P. G. Reinhard, E. Suraud, and C. A. Ullrich, Phys. Rep. **337**, 493 (2000).
[83] G. T. Velde, F. M. Bickelhaupt, E. J. Baerends, C. F. Guerra, S. J. A. Van Gisbergen, J. G. Snijders, and T. Ziegler, J. Comput. Chem. **22**, 931 (2001).
[84] G. Onida, L. Reining, and A. Rubio, Rev. Mod. Phys. **74**, 601 (2002).
[85] J. P. Perdew, in: Electronic Structure of Solids, edited by P. Ziesche and H. Eschrig (Akademie Verlag, Berlin, 1991), pp.11.
[86] K. Burke, J. P. Perdew and Y. Wang, in: Electronic Density Functional Theory: Recent Progress and New Directions, edited by J. F. Dobson, G. Vignale, and M.P. Das (Plenum, 1998).
[87] P. M. W. Gill, Mol. Phys. **89**, 433 (1996).
[88] C. Adamo and V. Barone, J. Chem. Phys. **108**, 664 (1998).
[89] C. Lee, W. Yang, and R. G. Parr, Phys. Rev. B **37**, 785 (1988).
[90] J. P. Perdew and A. Zunger, Phys. Rev. B **23**, 5048 (1981).
[91] A. D. Becke, J. Chem. Phys. **98**, 5648 (1993).
[92] J. C. Slater, Quantum Theory of Molecular and Solids,

Vol.4: The Self-Consistent Field for Molecular and Solids (McGraw-Hill, New York, 1974).
[93] S. H. Vosko, L. Wilk and M. Nusair, Can. J. Phys. **58**, 1200 (1980).
[94] M. W. Feyereisen, J. Nichols, J. Oddershede, and J. Simons, J. Chem. Phys. **96**, 2978 (1992).
[95] H. Weiss, R. Ahlrichs, and M. Häser, J. Chem. Phys. **99**, 1262 (1993).
[96] T. M. Henderson, K. Runge, and R. J. Bartlett, Phys. Rev. B **67**, 045320 (2003).
[97] I. Renge, J. Phys. Chem. **99**, 15955 (1995).
[98] W. Krätchmer, L. D. Lamb, K. Fostiropoulos, and D. R. Huffman, Nature (London) **347**, 345 (1990).
[99] H. W. Kroto, A. W. Allaf, and S. P. Balm, Chem. Rev. **91**, 1213 (1991).
[100] E. L. Shirley and S. G. Louie, Phys. Rev. Lett. **71**, 133 (1993); E. L. Shirley, L. X. Benedict, and S. G. Louie, Phys. Rev. B **54**, 10970 (1996).
[101] J. W. Arbogast, A. P. Darmanyan, C. S. Foote, Y. Rubin, F. N. Diederich, M. M. Alvarez, S. J. Anz, and R. L. Whetten, J. Phys. Chem. **95**, 11 (1991).
[102] D. M. Guldi, H. Hungerbühler, I. Carmichael, K. D. Asmus, and M. Maggini, J. Phys. Chem. A **104**, 8601 (2000).
[103] M. Braga, S. Larsson, A. Rosen, and A. Volosov, Astron. Astrophys. **245**, 232 (1991).
[104] N. M. Dimitrijević and P. Kamat, J. Phys. Chem. **96**, 4811 (1992).
[105] S. Weiss, Science **283**, 1676 (1999).
[106] T. Da Ros and M. Prato, Chem. Commun. 663 (1999).
[107] N. Tagmatarchis and H. Shinohara, Mini-Rev. Med. Chem. **1**, 339 (2001).

Table I: Calculated and measured $^{(1)}E_1$ (in eV), $^{(3)}E_1$, and the energy ϵ_i (in eV) of the ith dipole-allowed transition with an oscillator strength $f_{osc,i}$ for C_{60}. All TD-HF and TD-DFT use the minimum basis set STO-3G except the specified cases.

Methods	$^{(3)}E_1$	$^{(1)}E_1$	ϵ_1	$f_{osc,1}$	ϵ_2	$f_{osc,2}$
ZINDO/1600	1.190	2.234	3.221	0.0040	3.951	0.4663
ZINDO/2500	1.063	2.231	3.213	0.0050	3.933	0.4864
CINDO/S/900 [103]			3.40	0.080	4.04	0.410
TD-HF/3-21G	-2.799	3.056	5.510	0.8010	6.504	0.1010
TD-HF/6-31G+s [95]			5.22	0.890	6.19	0.060
TD-DFT-TB [70]	1.731	1.803	2.636	0.0020	3.350	0.1530
TD-LSDA	1.961	2.128	3.201	0.0016	4.026	0.1461
TD-BLYP	1.847	2.119	3.179	0.0018	3.981	0.1404
TD-BPL	1.866	2.117	3.171	0.0018	3.967	0.1393
TD-BP86	1.865	2.140	3.215	0.0017	4.027	0.1445
TD-BPW91	1.849	2.140	3.213	0.0017	4.025	0.1446
TD-PW91LYP	1.851	2.116	3.174	0.0017	3.977	0.1399
TD-PW91PL	1.870	2.114	3.167	0.0017	3.963	0.1389
TD-PW91P86	1.869	2.137	3.210	0.0017	4.023	0.1443
TD-PW91PW91	1.854	2.136	3.210	0.0017	4.021	0.1445
TD-MPWLYP	1.847	2.117	3.176	0.0017	3.978	0.1398
TD-MPWPL	1.866	2.115	3.168	0.0017	3.964	0.1391
TD-MPWP86	1.865	2.138	3.212	0.0017	4.024	0.1442
TD-MPWPW91	1.849	2.138	3.210	0.0017	4.022	0.1443
TD-G96LYP	1.838	2.121	3.182	0.0017	3.984	0.1406
TD-G96PL	1.858	2.119	3.175	0.0017	3.970	0.1395
TD-G96P86	1.856	2.142	3.218	0.0017	4.031	0.1450
TD-G96PW91	1.839	2.141	3.216	0.0017	4.029	0.1450
TD-B3LYP	1.882	2.591	3.931	0.0098	4.550	0.2456
TD-B3P86	1.889	2.606	3.956	0.0097	4.584	0.2505
TD-B3PW91	1.863	2.607	3.958	0.0096	4.587	0.2509
TD-B1LYP	1.796	2.707	4.119	0.0153	4.688	0.2732
TD-MPW1PW91	1.776	2.725	4.150	0.0150	4.729	0.2799
TD-B3LYP/3-21G	1.706	2.217	3.564	0.0115	4.082	0.2017
TD-LSDA/3-21G	1.691	1.822	2.916	0.0019	3.626	0.1206
TD-BP86/6-31G+s [54]			2.82	0.002	3.51	0.139
TD-BP86/3-21G	1.617	1.831	2.924	0.0019	3.623	0.1197
Exp./hexane [47]			3.03		3.78	
Exp./hexane [48]			3.07		3.77	
Exp./Ar-matrices [49]			3.06		3.80	
Exp./hexane [50]			3.04	0.015	3.78	0.37
Exp./cyclohexane [51]			3.07		3.77	
Exp./1-octanol [51]			3.06		3.76	
Exp./2-octanol [51]			3.07		3.77	
Exp./benzene [51]			3.05		3.70	
Exp./toluene [51]			3.05		3.70	
Exp./gas [52]			3.04		3.75	
Exp./hexane [53]			3.035	0.003	3.732	0.09
Exp./heptane [53]			3.035	0.003	3.732	0.09
Exp./toluene [53]			3.012		3.709	
Exp./hexane [54]			3.07		3.77	
Exp./benzene [66]	1.65	1.78	3.05		3.71	

Table II: Exciton pair contribution P_n^v (HOMO $-\,n$, LUMO $+\,v$, see definition in text), to the first singlet state ($^{(1)}E_1$) and the first two dipole-allowed singlet states (ϵ_1 and ϵ_2) calculated for C_{60}. The energy level ordering and symmetry of C_{60} in the ground state are represented in Fig.2. Except the specified case, all use the minimum basis set STO-3G. Π is the degeneracy of excited states.

Methods	$^{(1)}E_1(\Pi=4)$	$\epsilon_1(\Pi=3)$	$\epsilon_2(\Pi=3)$
TD-LSDA	49_0^0	$16_2^0+33_0^1$	$19_2^0+6_0^1+17_0^2$
TD-LSDA/3-21G	49_0^0	$16_2^0+34_0^1$	$20_2^0+5_0^1+0_0^2+16_0^3$
TD-BLYP	49_0^0	$15_2^0+31_0^1$	$18_2^0+5_0^1+12_0^2$
TD-BPL	50_0^0	$12_2^0+32_0^1$	$18_2^0+6_0^1+15_0^2$
TD-BP86	47_0^0	$15_2^0+33_0^1$	$19_2^0+6_0^1+17_0^2$
TD-BP86/3-21G	50_0^0	$15_2^0+33_0^1$	$19_2^0+5_0^1+16_0^3$
TD-BPW91	45_0^0	$15_2^0+32_0^1$	$18_2^0+6_0^1+14_0^2$
TD-PW91LYP	49_0^0	$15_2^0+33_0^1$	$18_2^0+6_0^1+17_0^2$
TD-PW91PL	49_0^0	$15_2^0+32_0^1$	$17_2^0+7_0^1+16_0^2$
TD-PW91P86	48_0^0	$16_2^0+33_0^1$	$18_2^0+7_0^1+16_0^2$
TD-PW91PW91	49_0^0	$16_2^0+33_0^1$	$18_2^0+4_0^1+12_0^2$
TD-MPWLYP	48_0^0	$15_2^0+32_0^1$	$18_2^0+6_0^1+18_0^2$
TD-MPWPL	49_0^0	$14_2^0+33_0^1$	$18_2^0+6_0^1+16_0^2$
TD-MPWP86	49_0^0	$13_2^0+33_0^1$	$19_2^0+6_0^1+16_0^2$
TD-MPWPW91	49_0^0	$15_2^0+33_0^1$	$19_2^0+5_0^1+16_0^2$
TD-G96LYP	49_0^0	$15_2^0+33_0^1$	$20_2^0+6_0^1+17_0^2$
TD-G96PL	48_0^0	$15_2^0+33_0^1$	$20_2^0+6_0^1+17_0^2$
TD-G96P86	47_0^0	$15_2^0+32_0^1$	$18_2^0+4_0^1+16_0^2$
TD-G96PW91	49_0^0	$16_2^0+33_0^1$	$18_2^0+4_0^1+16_0^2$
TD-B3LYP	49_0^0	$12_1^0+34_0^1$	$24_1^0+3_0^1+11_0^2$
TD-B3LYP/3-21G	50_0^0	$10_2^0+36_0^1$	$25_2^0+4_0^1+12_0^3$
TD-B3P86	48_0^0	$12_1^0+36_0^1$	$25_1^0+2_0^1+13_0^2$
TD-B3PW91	50_0^0	$11_1^0+35_0^1$	$24_1^0+4_0^1+13_0^2$
TD-B1LYP	50_0^0	$10_1^0+36_0^1$	$26_1^0+3_0^1+12_0^2$
TD-MPW1PW91	49_0^0	$10_1^0+37_0^1$	$26_1^0+3_0^1+12_0^2$

Table III: Exciton participation contribution P_n^v to the triplet states in the first two energy bands of C_{60} calculated with TD-BP86/3-21G. Π is the degeneracy of the excited state.

Band	States	E (eV)	Π	P_n^v
Band 1	$^{(3)}E_1$	1.617	3	55_0^0
	$^{(3)}E_2$	1.737	5	52_0^0
	$^{(3)}E_3$	1.750	3	52_0^0
	$^{(3)}E_4$	1.796	4	50_0^0
Band 2	$^{(3)}E_5$	2.601	4	$34_0^1 + 9_1^0 + 7_2^0$
	$^{(3)}E_6$	2.704	3	$46_0^1 + 6_2^0$
	$^{(3)}E_7$	2.725	3	$38_0^1 + 12_1^0$
	$^{(3)}E_8$	2.784	5	$45_0^1 + 5_1^0$
	$^{(3)}E_9$	2.905	3	$35_1^0 + 10_0^1 + 1_2^0$
	$^{(3)}E_{10}$	2.916	4	$28_1^0 + 16_0^1 + 2_2^0$
	$^{(3)}E_{11}$	2.925	5	$44_1^0 + 4_0^1$
	$^{(3)}E_{12}$	2.991	4	$37_2^0 + 12_1^0$
	$^{(3)}E_{13}$	3.000	3	$44_2^0 + 3_0^1$
	$^{(3)}E_{14}$	3.014	3	$46_2^0 + 1_1^0$
	$^{(3)}E_{15}$	3.026	5	48_2^0

Table IV: Main exciton pair contribution P_n^v to the first 15 triplet states, and dipole-allowed singlet states of $C_{59}N^+$ in the visible and UV regions calculated by TD-BP86/3-21G. E, λ and f_{osc} are the energy, wavelength and oscillator strength. The energy is not degenerated.

State	Symmetry	E (eV)	λ (nm)	f_{osc}	P_n^v
$^{(3)}E_1$	A''	1.351	917.56	0.0000	$34_0^0 + 13_1^0 + 6_3^0$
$^{(3)}E_2$	A''	1.375	901.92	0.0000	$36_1^0 + 15_0^0$
$^{(3)}E_3$	A'	1.405	882.60	0.0000	50_2^0
$^{(3)}E_4$	A''	1.421	872.65	0.0000	$45_3^0 + 3_1^0 + 3_0^0$
$^{(3)}E_5$	A'	1.509	821.66	0.0000	$44_4^0 + 4_3^1 + 3_1^1$
$^{(3)}E_6$	A''	1.585	782.45	0.0000	$43_2^1 + 5_0^2 + 4_1^2$
$^{(3)}E_7$	A'	1.602	774.07	0.0000	$34_1^1 + 11_3^1 + 6_4^0$
$^{(3)}E_8$	A'	1.617	766.92	0.0000	$44_0^1 + 4_3^1 + 2_1^1$
$^{(3)}E_9$	A'	1.641	755.51	0.0000	$32_3^1 + 12_1^1 + 6_0^1$
$^{(3)}E_{10}$	A''	1.673	740.91	0.0000	$31_0^2 + 17_1^2 + 3_4^1$
$^{(3)}E_{11}$	A''	1.711	724.72	0.0000	$31_1^2 + 13_0^2 + 8_2^1$
$^{(3)}E_{12}$	A'	1.788	693.30	0.0000	50_2^2
$^{(3)}E_{13}$	A''	1.792	692.02	0.0000	$47_4^1 + 2_0^2$
$^{(3)}E_{14}$	A''	1.813	683.94	0.0000	$49_3^2 + 2_0^2$
$^{(3)}E_{15}$	A'	1.925	644.18	0.0000	51_4^2
$^{(1)}E_1$	A''	1.487	834.00	0.0001	$39_1^0 + 8_0^0$
$^{(1)}E_2$	A''	1.518	816.72	0.0005	$38_3^0 + 9_0^0$
$^{(1)}E_3$	A'	1.546	802.02	0.0005	$45_2^0 + 1_1^1$
$^{(1)}E_5$	A'	1.675	740.28	0.0006	$44_4^0 + 2_1^1$
$^{(1)}E_{13}$	A'	1.947	636.67	0.0003	$40_2^2 + 4_3^1 + 1_4^2$
$^{(1)}E_{15}$	A'	2.090	593.19	0.0004	$44_4^2 + 1_2^2$
$^{(1)}E_{17}$	A'	2.663	465.50	0.0022	$44_6^0 + 2_1^5 + 1_1^4$
$^{(1)}E_{18}$	A''	2.681	462.50	0.0002	$39_8^0 + 7_0^3$
$^{(1)}E_{20}$	A'	2.716	456.47	0.0011	$35_7^0 + 5_0^5 + 3_2^3 + 2_9^0$
$^{(1)}E_{21}$	A''	2.733	453.65	0.0005	$25_0^3 + 11_1^3 + 8_{10}^0 + 2_8^0$
$^{(1)}E_{22}$	A'	2.759	449.44	0.0002	$44_9^0 + 2_2^3 + 1_7^0$
$^{(1)}E_{24}$	A'	2.792	444.02	0.0005	$31_2^3 + 5_0^4 + 3_{11}^0 + 2_7^0 + 2_1^5$
$^{(1)}E_{25}$	A''	2.794	443.83	0.0028	$36_{10}^0 + 4_{12}^0 + 2_8^0 + 2_0^3 + 2_1^3$
$^{(1)}E_{28}$	A'	2.864	432.90	0.0004	$19_1^4 + 8_1^5 + 4_8^1 + 4_0^4 + 2_5^1$
$^{(1)}E_{33}$	A''	2.912	425.79	0.0010	$22_{12}^0 + 10_7^1 + 6_6^1 + 6_2^5$
$^{(1)}E_{34}$	A''	2.920	424.66	0.0007	$26_7^1 + 12_2^4 + 5_2^5 + 3_{12}^0$
$^{(1)}E_{36}$	A''	2.954	419.72	0.0010	$18_9^1 + 9_6^1 + 9_2^5 + 6_5^2 + 4_{12}^0$
$^{(1)}E_{37}$	A'	2.967	417.93	0.0008	$11_{10}^1 + 6_0^5 + 5_3^4 + 5_1^5 + 4_6^2$
$^{(1)}E_{38}$	A'	2.984	415.52	0.0005	$16_{11}^0 + 14_{10}^1 + 5_6^2 + 4_7^2$
$^{(1)}E_{39}$	A'	2.986	415.20	0.0017	$20_4^3 + 9_3^4 + 4_7^2 + 3_{12}^1 + 3_6^3$
$^{(1)}E_{40}$	A''	3.007	412.28	0.0004	$32_4^4 + 7_5^2 + 5_4^5 + 2_8^2 + 1_{11}^1$
$^{(1)}E_{41}$	A''	3.023	410.12	0.0003	$27_4^5 + 12_9^1 + 6_5^2 + 1_{11}^1 + 1_{10}^2$
$^{(1)}E_{42}$	A'	3.067	404.31	0.0014	$18_6^2 + 14_9^2 + 6_0^5 + 2_{10}^1 + 2_8^1 + 2_7^0$
$^{(1)}E_{43}$	A''	3.085	401.90	0.0003	$39_8^2 + 6_{11}^1 + 1_{10}^2$
$^{(1)}E_{44}$	A''	3.087	401.69	0.0008	$34_7^2 + 3_{12}^1 + 3_{10}^1 + 1_4^3 + 1_3^4$
$^{(1)}E_{58}$	A'	3.508	353.44	0.0351	$24_4^6 + 6_{13}^0 + 3_9^2$
$^{(1)}E_{59}$	A'	3.588	345.57	0.0524	$19_4^6 + 7_{13}^2 + 3_{11}^2 + 2_2^7$
$^{(1)}E_{60}$	A''	3.677	337.21	0.0461	$18_{13}^1 + 10_0^7 + 3_3^7 + 2_1^{10}$
$^{(1)}E_{61}$	A'	3.687	336.31	0.1017	$5_2^6 + 5_9^2 + 4_{13}^0 + 3_3^9 + 3_4^7 + 3_1^9 + 2_{10}^1 + 2_4^6 + 2_1^{11}$

Table V: Exciton pair contribution P_n^v to the first three triplet bands, and several representative dipole-allowed singlet states for the most stable isomer I of $C_{48}N_{12}$ calculated by TD-BP86/3-21G. E, λ and Π are the energy, wavelength and degeneracy of excited states.

State	E (eV)	λ (nm)	Π	f	P_n^v
$^{(3)}E_1$	1.547	801.61	2	0.0000	52_0^0
$^{(3)}E_2$	1.743	711.29	1	0.0000	52_0^1
$^{(3)}E_3$	1.769	701.07	1	0.0000	$32_0^1 + 20_0^2$
$^{(3)}E_4$	1.809	685.24	2	0.0000	50_0^1
$^{(3)}E_5$	1.830	677.41	1	0.0000	51_0^1
$^{(3)}E_6$	1.849	670.53	1	0.0000	$33_0^2 + 18_1^0$
$^{(3)}E_7$	1.874	661.55	2	0.0000	51_0^2
$^{(3)}E_8$	1.916	646.96	1	0.0000	$49_0^2 + 2_1^0$
$^{(3)}E_9$	2.062	601.22	2	0.0000	$43_1^1 + 8_2^0$
$^{(3)}E_{10}$	2.191	566.02	2	0.0000	51_1^2
$^{(3)}E_{11}$	2.240	553.42	2	0.0000	$41_2^0 + 8_1^1$
$^{(1)}E_1$	1.698	730.23	2	0.0003	47_0^0
$^{(1)}E_6$	2.024	612.62	1	0.0041	$28_1^0 + 17_0^2$
$^{(1)}E_7$	2.120	584.82	2	0.0179	$40_0^2 + 5_1^2$
$^{(1)}E_8$	2.126	583.32	1	0.0044	45_0^2
$^{(1)}E_{10}$	2.348	528.15	2	0.0083	$42_1^2 + 2_0^2$
$^{(1)}E_{13}$	2.617	473.85	1	0.0028	48_2^1
$^{(1)}E_{18}$	2.716	456.45	2	0.0299	$40_2^1 + 3_0^6$
$^{(1)}E_{21}$	2.802	442.45	1	0.0521	40_2^1
$^{(1)}E_{30}$	3.254	381.00	2	0.0099	$25_0^6 + 18_2^3$
$^{(1)}E_{31}$	3.288	377.08	2	0.0075	$26_2^3 + 14_4^1 + 9_2^4 + 8_0^6$
$^{(1)}E_{34}$	3.388	365.92	1	0.0021	$39_2^4 + 8_4^1$
$^{(1)}E_{36}$	3.412	363.37	2	0.0066	$32_2^4 + 9_4^1 + 2_2^3 + 2_1^6 + 2_0^6$
$^{(1)}E_{37}$	3.465	357.84	1	0.0010	$43_1^6 + 2_0^7$
$^{(1)}E_{38}$	3.497	354.53	1	0.0019	46_4^1
$^{(1)}E_{39}$	3.535	350.72	1	0.0164	$27_4^1 + 11_0^8 + 4_3^3 + 2_2^4$
$^{(1)}E_{40}$	3.543	349.94	2	0.0032	$39_0^7 + 2_0^8$
$^{(1)}E_{42}$	3.643	340.38	2	0.0293	$16_0^8 + 13_4^1 + 10_3^4 + 2_2^5$
$^{(1)}E_{46}$	3.700	335.21	2	0.0266	$21_0^8 + 7_2^5 + 6_4^1 + 6_3^4 + 1_1^8$
$^{(1)}E_{49}$	3.739	331.63	2	0.0202	$22_2^5 + 12_3^4 + 5_4^1 + 4_0^8$
$^{(1)}E_{50}$	3.787	327.42	1	0.0256	$17_1^7 + 15_0^8 + 7_3^3 + 4_4^1$
$^{(1)}E_{51}$	3.824	324.26	2	0.0241	$17_3^4 + 9_2^5 + 8_5^1 + 3_1^8 + 1_0^7$
$^{(1)}E_{55}$	3.953	313.65	1	0.0575	$18_1^8 + 8_3^5 + 5_0^8 + 4_3^3 + 2_4^4$
$^{(1)}E_{59}$	4.005	309.59	1	0.0013	$21_5^1 + 13_1^8 + 6_4^3 + 2_2^5 + 1_0^{10}$
$^{(1)}E_{62}$	4.097	302.64	2	0.0495	$24_1^8 + 9_5^1 + 2_7^0 + 2_4^3$
$^{(1)}E_{63}$	4.181	296.53	1	0.0013	$30_4^3 + 10_0^{10} + 4_4^4 + 1_5^1$
$^{(1)}E_{65}$	4.209	294.59	1	0.0016	$23_3^5 + 21_4^4$
$^{(1)}E_{67}$	4.273	290.13	2	0.0010	$30_0^{10} + 6_4^3 + 4_4^4 + 2_5^1$

Table VI: Exciton pair contribution P_n^v to the first five triplet bands, and several representative dipole-allowed singlet states for the stable isomer II of $C_{48}N_{12}$ calculated by TD-BP86/3-21G. E, λ and Π are the energy, wavelength and degeneracy of excited states.

State	E (eV)	λ (nm)	Π	f	P_n^v
$^{(3)}E_1$	0.806	1539.22	2	0.0000	55_0^0
$^{(3)}E_2$	1.115	1111.74	1	0.0000	$54_0^1 + 5_1^0$
$^{(3)}E_3$	1.208	1026.09	2	0.0000	52_0^1
$^{(3)}E_4$	1.255	988.24	1	0.0000	51_0^1
$^{(3)}E_5$	1.507	822.58	1	0.0000	54_0^2
$^{(3)}E_6$	1.550	800.02	1	0.0000	$48_1^0 + 3_0^1$
$^{(3)}E_7$	1.555	797.33	2	0.0000	52_0^2
$^{(3)}E_8$	1.596	777.00	1	0.0000	51_0^2
$^{(3)}E_9$	1.805	687.01	2	0.0000	50_0^3
$^{(3)}E_{10}$	1.854	668.87	1	0.0000	51_2^0
$^{(3)}E_{11}$	1.918	646.28	2	0.0000	51_1^1
$^{(3)}E_{12}$	2.025	612.21	2	0.0000	$46_3^0 + 3_0^4$
$^{(3)}E_{13}$	2.054	603.49	1	0.0000	52_0^4
$^{(3)}E_{14}$	2.098	590.95	2	0.0000	$46_0^4 + 3_3^0 + 1_1^2$
$^{(3)}E_{15}$	2.136	580.33	1	0.0000	51_0^4
$^{(1)}E_1$	0.997	1243.20	2	0.0037	44_0^0
$^{(1)}E_7$	1.750	708.30	2	0.0048	46_2^0
$^{(1)}E_8$	1.809	685.46	1	0.0187	$42_0^2 + 1_2^0 + 1_1^3$
$^{(1)}E_{10}$	2.087	594.12	2	0.0067	45_1^1
$^{(1)}E_{11}$	2.091	592.87	1	0.0077	43_2^0
$^{(1)}E_{18}$	2.552	485.82	1	0.0012	$44_3^1 + 3_1^3$
$^{(1)}E_{19}$	2.617	473.78	2	0.0087	$35_3^1 + 6_2^2 + 6_0^5$
$^{(1)}E_{20}$	2.652	467.46	1	0.0010	$40_3^1 + 2_1^3 + 4_0^5$
$^{(1)}E_{21}$	2.752	450.61	1	0.0137	$34_1^3 + 4_0^5 + 4_0^7 + 2_3^1$
$^{(1)}E_{22}$	2.757	449.76	2	0.0023	$39_2^2 + 8_0^5$
$^{(1)}E_{23}$	2.859	433.62	1	0.0078	44_0^5
$^{(1)}E_{24}$	2.901	427.37	2	0.0027	$38_1^4 + 9_0^5$
$^{(1)}E_{28}$	2.982	415.84	1	0.0164	$37_0^5 + 2_4^1 + 2_1^3 + 1_1^6$
$^{(1)}E_{31}$	3.111	398.54	2	0.0339	$28_0^7 + 5_3^3 + 4_1^4 + 10_0^5$
$^{(1)}E_{33}$	3.153	393.28	2	0.0016	$30_3^3 + 16_0^7$
$^{(1)}E_{35}$	3.218	385.30	1	0.0071	$38_0^7 + 6_4^1$
$^{(1)}E_{37}$	3.289	376.96	2	0.0784	$11_3^3 + 8_0^7 + 4_4^1 + 6_0^5 + 4_3^4 + 3_1^4$
$^{(1)}E_{39}$	3.460	358.34	2	0.0115	$24_4^1 + 16_3^4 + 4_0^8$
$^{(1)}E_{42}$	3.500	354.65	2	0.0191	$22_3^4 + 18_4^1 + 2_0^8$
$^{(1)}E_{43}$	3.573	347.02	2	0.0118	$39_0^8 + 4_3^4$
$^{(1)}E_{50}$	3.817	324.84	1	0.1630	$18_4^1 + 14_7^0 + 5_3^4$
$^{(1)}E_{52}$	3.861	321.16	2	0.0031	$32_0^{10} + 14_2^5$
$^{(1)}E_{53}$	3.870	320.35	1	0.0014	$38_1^6 + 4_5^1 + 2_9^0 + 1_7^0$
$^{(1)}E_{56}$	3.932	315.35	2	0.0010	$29_2^5 + 12_0^{10} + 1_3^6$
$^{(1)}E_{58}$	4.018	308.56	2	0.0010	$41_0^{12} + 5_5^1 + 1_6^0 + 1_4^3$
$^{(1)}E_{63}$	4.085	303.54	2	0.0051	$33_4^3 + 7_6^0 + 3_2^7 + 2_0^{12} + 1_1^9$
$^{(1)}E_{64}$	4.125	300.59	1	0.0010	$38_5^1 + 3_0^{13} + 2_9^0$
$^{(1)}E_{65}$	4.136	299.77	2	0.0203	$17_5^1 + 13_6^0 + 6_0^{13} + 3_4^4 + 2_4^3$